Synthesis and Characterization of Linear Low-Density Polyethylene/Sepiolite Nanocomposites

Muhammad Shafiq, Tariq Yasin, Shaukat Saeed

Department of Chemical and Materials Engineering, Pakistan Institute of Engineering and Applied Sciences, Nilore, Islamabad, Pakistan

Received 19 November 2010; accepted 5 April 2011
DOI 10.1002/app.34633
Published online 19 August 2011 in Wiley Online Library (wileyonlinelibrary.com).

ABSTRACT: Linear low-density polyethylene (LLDPE)/sepiolite nanocomposites were prepared by melt blending using unmodified and silane-modified sepiolite. Two methods were used to modify sepiolite: modification before heat mixing (*ex situ*) and modification during heat mixing (*in situ*). The X-ray diffraction results showed that the position of the main peak of sepiolite remained unchanged during modification step. Infrared spectra showed new peaks confirming the development of new bonds in modified sepiolite and nanocomposites. SEM micrographs revealed the presence of sepiolite fibers embedded in polymer matrix. Thermogravimetric analysis showed that nanocomposites exhibited higher onset degradation temperature than LLDPE. In addition, *in situ* modified sepiolite nanocomposites exhibited higher thermal stability than ex *situ* modified sepiolite nanocomposites. The ultimate tensile strength and modulus of the nanocomposites were improved; whereas elongation at break was reduced. The higher crystallization temperature of some nanocomposite formulations revealed a heterogeneous nucleation effect of sepiolite. This can be exploited for the shortening of cycle time during processing. © 2011 Wiley Periodicals, Inc. J Appl Polym Sci 123: 1718–1723, 2012

Key words: nanocomposites; thermal properties; LLDPE; sepiolite

INTRODUCTION

Polymer/clay nanocomposites have attracted wide interest in recent years for exhibiting improved mechanical, thermal, barrier, and optical properties.[1–3] The nano-sized additive exhibits large surface area, which enhances the interfacial interaction between polymer and additive, which in turn improves the properties of the nanocomposites. Even small loading of nano particle imparts excellent properties.[4–6] A great fractions of published data on polymer/clay nanocomposites focused on lamellar layered silicates, especially on the intercalation and exfoliation of montmorillonite, whereas polymer/sepiolite nanocomposites have not been studied to that extent.[1]

Sepiolite is also a member of the phyllosilicate mineral family. It is hydrated magnesium silicate clay having microfibrous morphology and its structure consists of an octahedral sheet of magnesia sandwiched between two tetrahedral silica sheets. The result of discontinuity of octahedral sheets in sepiolite exposes number of silanol groups (Si—OH) on its external surface. These groups can enhance the interfacial interaction between polymer and sepiolite and can also be used for its functionalization and/or modification.[7–10] Sepiolite has been used for the preparation of nanocomposites using different polymers as matrix.[11–15] Limited work has been reported on polyethylene/sepiolite nanocomposites.

The key issue in polyolefins/sepiolite nanocomposites is to develop good compatibility between hydrophobic polymer and hydrophilic sepiolite. To address this issue, either the modified sepiolite or functional polymers are employed. In the present work, the effect of addition of unmodified and silane modified sepiolite on the properties of LLDPE/sepiolite nanocomposites was investigated. A novel approach has been used to modify sepiolite with silane. Vinyl triethoxy silane (VTES) has been used due to these advantages: its silanol groups react with the hydroxyl groups of sepiolite and its vinyl moiety reacts with the polymer matrix. LLDPE has been selected due to its vast applications as cable insulation material, film and sheet formation, etc. Unmodified, *ex situ and in situ* silane modified sepiolite were heat mixed with LLDPE and compressed into sheets. The developed nanocomposites were characterized by FTIR, XRD, and SEM techniques. The comparison of thermal properties of these nanocomposites showed heterogeneous nucleation effect of sepiolite, which can be used for the shortening of cycle time during processing.

Correspondence to: T. Yasin (yasintariq@yahoo.com).

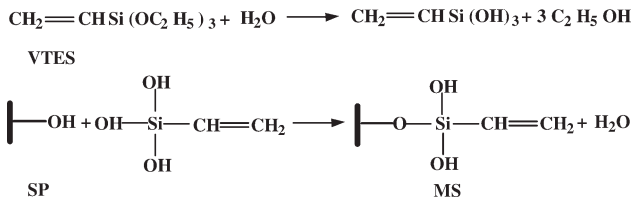

Scheme 1 Possible chemical reaction of SP with VTES.

EXPERIMENTAL

Materials

Linear low-density polyethylene (LL6201; density = 0.926 g/cm^3; melt flow index = 50 g/10 min) was purchased from Exxon Mobil Chemical (Riyadh, Saudi Arabia). Sepiolite (SP), vinyl triethoxy silane (VTES), dicumyl peroxide (DCP), and dibutyl tin dilaurate (DBTDL) were obtained from Sigma-Aldrich Chemie, Steinheim, Germany. SP was purified using the following procedure.[16] The suspension containing 10 g/L of SP was mechanically stirred for 24 h. After 2 min, supernatant suspension was filtered and the solid sample was dried at 105°C for 24 h. The dried samples were grounded sieved by 50 μm sieved and were used in all experiments. All other materials were used as such without further purification.

Sample preparation

The purified SP was modified (*ex situ*) with VTES using published method.[17] First, the SP was dispersed in isopropanol using mechanical stirring in a glass reactor, then the appropriate amount of VTES was added slowly into it at room temperature. The mixture was stirred for 2 h at 60°C. The resulting solid was recovered by filtration and washed with methanol. The *ex situ* modified sepiolite (MS) was dried overnight at 50°C under vacuum. A possible modification of sepiolite with VTES is shown in the following Scheme 1:

The LLDPE/sepiolite nanocomposites were prepared by heat mixing in Thermo Haake Polylab Rheomix internal mixer (Karlsruhe, Germany) using roller rotors. In the uncrosslinked formulations, LLDPE and SP were mixed at 170°C for 20 min. To prepare crosslinked formulations, first DCP was dissolved in acetone and sprayed over LLDPE powder. After the removal of acetone, the LLDPE was melted at 130°C and VTES, DBTDL, and sepiolite were added. Later, the temperature was raised to 170°C for 20 min. The rotor speed was kept constant at 60 rpm. The aforementioned admixtures were heat pressed at 150°C into sheets at 200 bars. The crosslinking of *in situ* modified sepiolite formulations was performed in water bath at 90°C for 7 h. The compositions of the prepared formulations are shown in Table I.

Characterization

The structural analysis of LLDPE and nanocomposites was performed with Fourier transform infrared (FTIR) spectroscopy. The FTIR spectra of the samples were recorded in attenuated total reflectance mode using a FTIR spectrophotometer (Model: Nicolet 6700, Thermo Electron Corporation, Waltham, MA), at a constant spectral resolution of 4 cm^{-1} in the range of 4000–400 cm^{-1} after acquiring 116 scans.

The morphology of the nanocomposites was examined using scanning electron microscopy (SEM) from Jeol (Model: JSM-6490LA, Japan). The cryo-fractured samples were sputter coated with gold and analyzed.

X-ray diffraction patterns were recorded using X-ray diffractometer (Model: X′ TRA48 Thermo ARL) using Cu Kα radiation (k = 0.15406 nm) operating at 45 kV and 40 mA. Radial scans were performed in reflection scanning mode with 2θ values ranging from 3 to 60° at a scanning rate of 1°/min.

Thermogravimetric analyzer from Mettler Toledo (Model: TGA/SDTA851^e, Schwerzenbaclz, Switzerland) was used to investigate the thermal stabilities of samples. A typical sample of ~ 10 mg was placed in alumina crucible and test was performed under flowing N_2 environment from 50 to 600°C at 20°C/min ramp.

Melting and crystallization behavior of the nanocomposites were studied using a differential scanning

TABLE I
Identification Codes and Formulation of LLDPE and Its Composites

Sample code	SP (phr)	MS (phr)	DCP (phr)	DBTDL (phr)	VTES (phr)
LL (LLDPE)	–	–	–	–	–
LS1 (unmodified sepiolite)	1	–	–	–	–
LS2 (unmodified sepiolite)	2	–	–	–	–
LVS1 (*in situ* modified sepiolite)	1	–	0.3	0.05	3
LVS2 (*in situ* modified sepiolite)	2	–	0.3	0.05	3
LMS1 (*ex situ* modified sepiolite)	–	1	0.3	–	–
LMS2 (*ex situ* modified sepiolite)	–	2	0.3	–	–

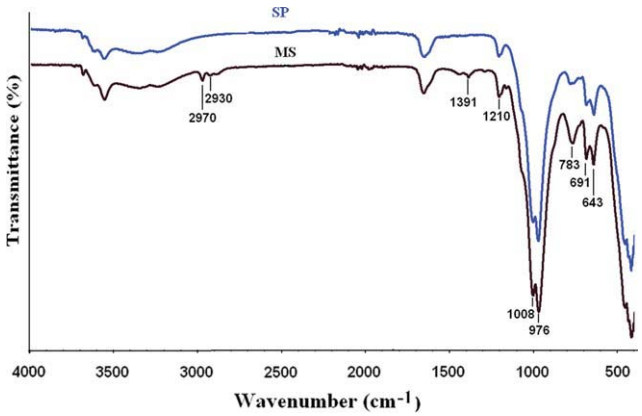

Figure 1 FTIR spectra of SP and MS in the range of 4000–400 cm^{-1} at 4 cm^{-1} resolution. [Color figure can be viewed in the online issue, which is available at wileyonlinelibrary.com.]

calorimeter (DSC) from TA Instruments (Model: Q100, New castle). The samples were sealed in an aluminum pans and both heating and cooling were carried out at 10°C/min under flowing N_2 (50 mL/min). The sample was first heated from ambient temperature to 180°C to erase thermal history, followed by cooling from 180°C to 50°C and then heated again to 180°C. The peak crystallization temperature (T_c) and the peak melting temperature (T_m) were determined from second and third scan respectively. Percent crystallinity (X_c) was calculated implying standard method using 289 J/g heat of fusion for 100% crystalline LLDPE according to the following equation[18]:

$$X_c = (\Delta H_f/289) \times 100$$

Vicat softening temperature (VST) was measured to assess the softening temperature of LLDPE and LLDPE/sepiolite nanocomposites. CEAST HDT junior instrument (Ceast SPA, Torino, Italy) with silicon oil bath at a heating rate of 50°C/h and load of 1 kg was used for measurements. The dimensions of the specimens used for the test were according to ASTM D1525.

Tensile properties were measured using a tensile testing machine (Model: BSS-500 kg, SANS, Transcell Technology, Shenzhen, China) according to ASTM D412-1998a. All tensile tests were performed at room temperature.

RESULTS AND DISCUSSION

The effect of addition of sepiolite (in different forms) on the properties of LLDPE/sepiolite nanocomposites was investigated. The structural and morphological analyses of nanocomposites were performed with FTIR, XRD, and SEM. Thermal analysis was performed with TGA and DSC.

Structural analysis

Infrared spectroscopy was performed to assess any physical or chemical interaction between SP, MS, and nanocomposites. FTIR spectra of SP and MS are shown in Figure 1. The spectrum of SP shows the O—H characteristic bands attributed to various types of water in the region of (3700–3300 cm^{-1}) and (800–650 cm^{-1}). The stretching vibration of Si—O is appeared at 1210, 1008, 976 cm^{-1} and its bending vibration at 460 cm^{-1}. The Si—O—Mg band is observed at 440 cm^{-1}.[8,17] The MS spectrum also showed new bands attributed to C—H group at 2970, 2930, and 1391 cm^{-1}, which confirm the chemical reaction of SP with VTES.

The FTIR spectra of LLDPE and LLDPE/sepiolite nanocomposites are shown in Figure 2. The characteristic bands of LLDPE associated with the C—H stretching vibration are observed at 2913 and 2847 cm^{-1}. The bending vibrations of ($—CH_2$) and ($—CH_3$) are appeared at 1461 and 1378 cm^{-1} respectively. The FTIR spectra of nanocomposites showed the combination of LLDPE and sepiolite. The nanocomposites exhibited the presence of spectral bands from both LLDPE and sepiolite. The intensity of the Si—O bands appeared in the region of 1100–1000 cm^{-1} in nanocomposites confirmed the added effect of siloxane linkage into sepiolite structure.

Morphological analysis

The morphological analysis of nanocomposites was performed with SEM. Figure 3 shows the micrographs of cryo-fractured surface of LS2, LMS2, and LVS2 nanocomposites. The micrographs of LS2 (A) and LMS2 (B) revealed the presence of sepiolite fibers embedded in the polymer matrix. Whereas LVS2 micrograph (C) showed that the sepiolite fibers were completely coated with polymer due to incorporation of silane coupling agent. This phenomenon

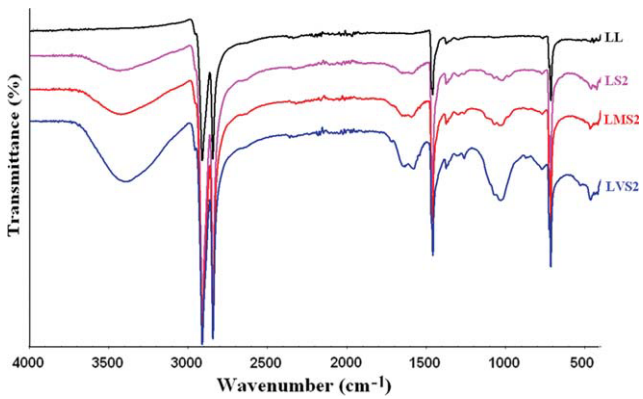

Figure 2 FTIR spectra of LLDPE and LLDPE/sepiolite nanocomposite in the range of 4000–400 cm^{-1} at 4 cm^{-1} resolution. [Color figure can be viewed in the online issue, which is available at wileyonlinelibrary.com.]

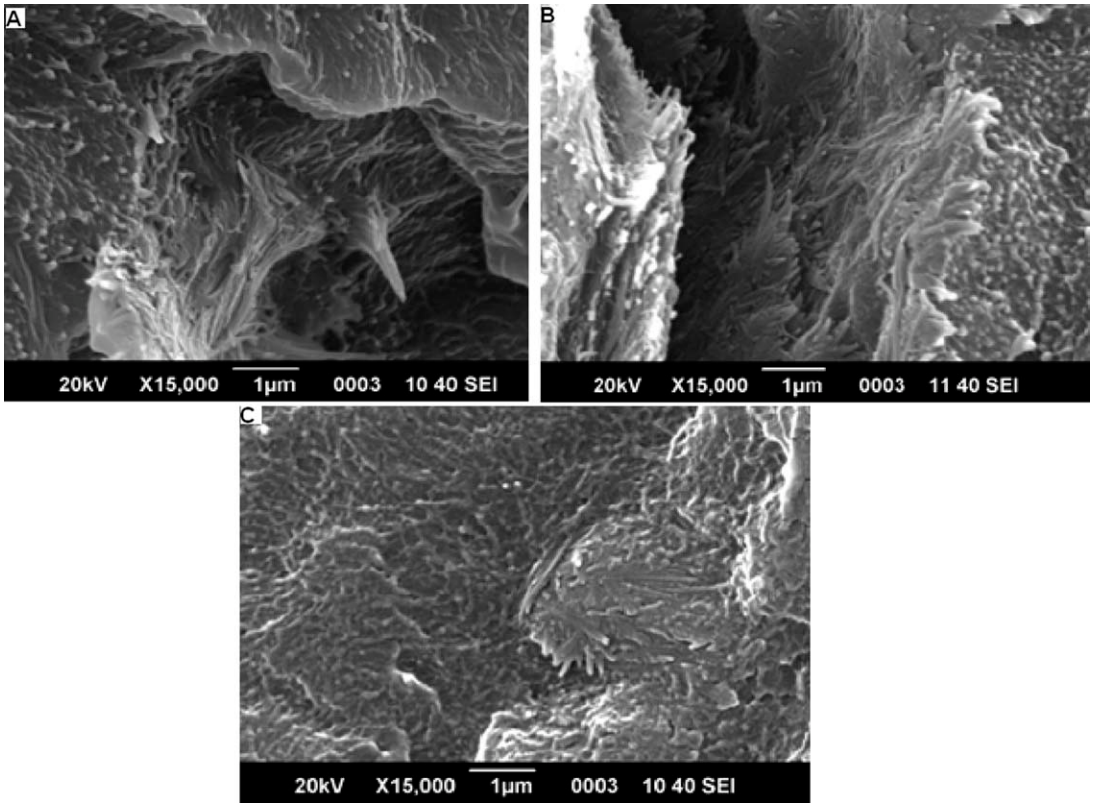

Figure 3 SEM micrographs of LS2 (A), LMS2 (B), and LVS2 (C) nanocomposites at ×15,000.

also confirmed that the *in situ* addition of VTES has improved the adhesion/crosslinking between LLDPE and sepiolite.

X-ray diffraction

The XRD patterns of SP and MS are shown in Figure 4. The SP has diffraction peaks at 7.2° (d_{110} = 1.22 nm) and 26.75° (d_{261} = 0.33 nm). The peak at 7.2° is related to the (110) crystalline plane of SP.[10] MS showed same peak positions with identical *d* spacings. This indicates that during modification step only the surface hydroxyl groups react with silanol and the main molecular structure of SP is remained unaffected.[17]

Figure 5 shows the XRD patterns of LLDPE and its nanocomposites. The peaks for LLDPE sample appeared at 21.49° (d_{110} = 0.41 nm) and 23.73° (d_{220} = 0.37 nm), which represent the orthorhombic unit

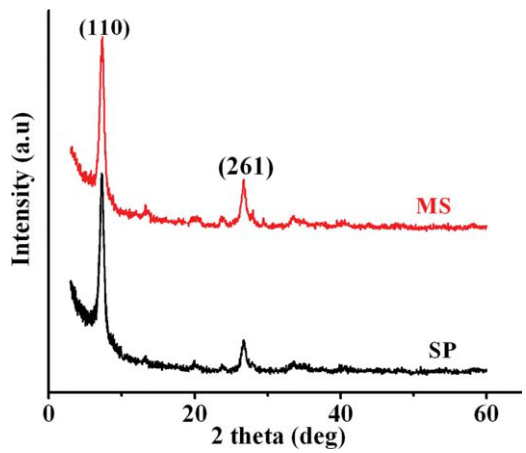

Figure 4 XRD patterns of SP and MS with 2θ values from 3 to 60°. [Color figure can be viewed in the online issue, which is available at wileyonlinelibrary.com.]

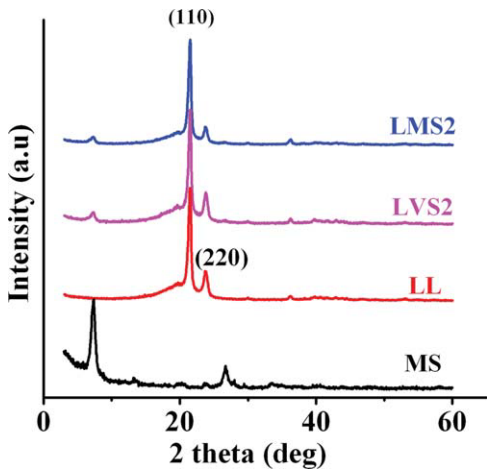

Figure 5 XRD patterns of LLDPE and LLDPE/sepiolite nanocomposites with 2θ values from 3 to 60°. [Color figure can be viewed in the online issue, which is available at wileyonlinelibrary.com.]

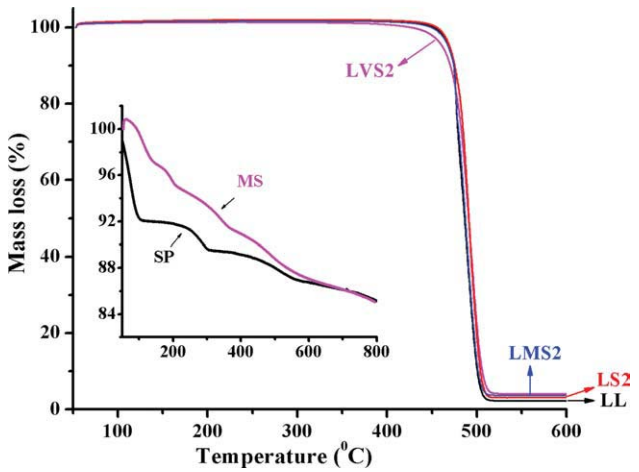

Figure 6 TGA curves of SP, MS, LLDPE, and LLDPE/sepiolite nanocomposites. [Color figure can be viewed in the online issue, which is available at wileyonlinelibrary.com.]

cell.[19] The nanocomposites also exhibited LLDPE and SP peaks at same positions as for pure samples. The strong diffraction peak of SP appeared as a small peak at 7.2° in the nanocomposites due to its small amount.[10]

Thermogravimetric analysis

Thermogravimetric analysis is performed to investigate the thermal stabilities of LLDPE and nanocomposites. Figure 6 shows the thermograms of SP, MS, LLDPE, and LLDPE/sepiolite nanocomposites. The corresponding mass loss data is summarized in Table II. SP shows step-wise mass loss with increase in temperature. It has been reported that this step-wise mass loss in SP is due to the loss of adsorbed and zeolitic water, the loss of the first structural water, the loss of the second structural water, and the release of water through dehydroxylation.[20] MS shows higher thermal stability as compared to SP and its mass loss is not in steps. This might be due to the reaction of SP with VTES as already discussed in Scheme 1. However, the total mass loss in both samples is 15.0 wt % at 800°C.

TABLE II
Thermogravimetric Analysis of LLDPE and Nanocomposites at Different Mass Losses

Sample code	T_{onset} (°C)	$T_{5\%}$ (°C)	$T_{50\%}$ (°C)	$T_{80\%}$ (°C)	Residue (%)
LL	451.9	468.5	485.9	496.1	2.3
LS2	464.3	470.1	491.5	499.0	3.0
LVS2	453.4	461.6	490.9	501.8	4.0
LMS2	460.6	467.4	487.4	497.7	3.7

T_{onset}, onset decomposition temperature; $T_{5\%}$, 5% decomposition temperature; $T_{50\%}$, 50% decomposition temperature; $T_{80\%}$, 80% decomposition temperature.

The thermograms of LLDPE and its nanocomposites exhibit similar degradation behaviour. The onset of degradation temperature (T_{onset}) of all nanocomposites is higher than LLDPE. In comparison with LLDPE, an increase of 12.4°C in LS2 and 8.7°C in LMS2 is observed. LVS2 shows higher thermal stability than LMS2. The higher stability of LVS2 can be explained as SP has more chances to develop chemical linkages with VTES and LLDPE during heat mixing and curing.

Differential scanning calorimetric analysis

The melting and crystallization behavior of LLDPE and nanocomposites was studied using DSC. The values of melting temperature (T_m), crystallization temperature (T_c), and percent crystallinity (X_c) are given in Table III. It can be seen from this table that the T_m increased from 123.8°C for LLDPE to a maximum of 126.2°C for LS2 with the incorporation of sepiolite. The T_c of LS2 and LMS2 shifted towards higher temperature. An increase of 1.7°C in T_c is observed in LMS2 which shows that the dispersion of SP and MS created heterogeneous nucleation sites in LLDPE. Whereas, LVS2 has shown a lower T_c and X_c than LLDPE and LMS2. The increased crystallization temperature of LS2 and LMS2 revealed a heterogeneous nucleation effect of sepiolite which can be exploited for the shortening of cycle time during processing.

VST

The VST indicates the softening temperature when a material is subjected to high temperature. The VST of LLDPE and LLDPE/sepiolite nanocomposites is summarized in Table III. Higher VST is exhibited by all nanocomposites than LLDPE and this increase is attributed to the presence of sepiolite. The VST of LVS2 is 8.9°C higher than LMS2 and this improvement also confirmed the presence of crosslinking network as previously discussed.

Mechanical properties

The mechanical properties were studied using tensile testing machine. Ultimate tensile strength (UTS),

TABLE III
Crystallization and Melting Characteristics of LLDPE and LLDPE/Sepiolite Nanocomposites

Sample	T_m (°C)	T_c (°C)	X_c (%)	VST (°C)
LL	123.8	109.2	30.3	85.0
LS2	126.2	110.0	31.0	88.5
LMS2	124.9	110.9	35.4	88.0
LVS2	125.6	106.1	27.3	96.9

TABLE IV
Mechanical Properties of LLDPE and LLDPE/Sepiolite Nanocomposites

Sample	LL	LS1	LS2	LVS1	LVS2	LMS1	LMS2
UTS (MPa)	12.5 ± 0.4	13.8 ± 0.3	15.0 ± 1.0	14.1 ± 0.4	17.7 ± 0.5	13.4 ± 0.2	14.5 ± 0.2
Eb (%)	105.0 ± 2	10.0 ± 1	4.6 ± 1	21.2 ± 1	22 ± 1	8.0 ± 1	7.4 ± 1
Modulus (MPa)	269 ± 4	321 ± 4	377 ± 5	320 ± 1	334 ± 4	344 ± 2	352 ± 3

elongation at break (Eb), and Young's modulus data are summarized in Table IV. It can be seen that, the UTS and modulus of the nanocomposites are higher than LLDPE. The LVS nanocomposites showed better UTS than LMS nanocomposites. The increasing trend of UTS from LVS1 to LVS2 is due to better interfacial bonding developed between SP and LLDPE. The Eb of nanocomposites decreases drastically as compared to LLDPE because of SP, which restricts the mobility of chains. The higher UTS and Eb of LVS nanocomposites than LLDPE and LMS nanocomposites is due to better adhesion of SP with LLDPE as revealed by SEM micrographs.

CONCLUSIONS

LLDPE/sepiolite nanocomposites containing unmodified, *ex situ* and *in situ* silane modified sepiolite have been prepared. The FTIR spectra of nanocomposites showed the presence of spectral bands from both LLDPE and sepiolite. The increased intensity of the Si—O bands in the region of 1100–1000 cm^{-1} in nanocomposites confirmed the added effect of siloxane linkage into sepiolite structure. SEM micrographs of nanocomposites revealed the presence of sepiolite fibers embedded in polymer matrix. Increased crystallization temperature of unmodified and *ex situ* modified sepiolite nanocomposites revealed a heterogeneous nucleation effect of sepiolite which can be exploited for the shortening of cycle time during processing. The VST of *in situ* modified sepiolite nanocomposites is higher than LLDPE and *ex situ* modified sepiolite nanocomposites, which confirmed the presence of crosslinking network. The higher UTS and Eb of *in situ* modified sepiolite nanocomposites than LLDPE and *ex situ* modified sepiolite nanocomposites is due to better adhesion of SP with LLDPE as revealed by SEM.

References

1. Fukushima, K.; Tauboani, D.; Camino, G. Mater Sci Eng C 2009, 29, 1433.
2. Paul, D. R.; Robeson, L. M. Polym 2008, 49, 3187.
3. Ray, S. S.; Okamoto, M. Prog Polym Sci 2003, 28, 1539.
4. Pavlidou, S.; Papaspyrides, C. D. Prog Polym Sci 2008, 33, 1119.
5. Pluta, M.; Galeski, A.; Alexandre, M.; Paul, M. A.; Dubois, P. J Appl Polym Sci 2002, 86, 1497.
6. Bilotti, E.; Fischer, H. R.; Peijs, T. J Appl Polym Sci 2008, 107, 16.
7. Zheng, Y.; Zheng, Y. J Appl Polym Sci 2006, 99, 2163.
8. Chen, H.; Zheng, M.; Sun, H.; Jia, Q. Mater Sci Eng A 2007, 15, 725.
9. Benlikaya, R.; Alkan, M.; Kaya, I. Polym Compos 2009, 30, 1586.
10. Tartaglione, G.; Tabuni, D.; Camino, G.; Moiso, M. Compos Sci Technol 2008, 68, 451.
11. Arroyo, M.; Perez, F.; Vigo, J. P. J Appl Polym Sci 1986, 32, 5105.
12. Huang, N. H.; Chen, Z. J.; Yi, C. H.; Wang, J. Q. eXPRESS Polym Lett 2010, 4, 227.
13. Darder, M.; Blanco, M. L.; Aranda, P.; Aznar, A. J.; Bravo, J.; Hitzky, A. R. Chem Mater 2006, 18, 1602.
14. Alkan, M.; Benlikaya, R. J Appl Polym Sci 2009, 112, 3764.
15. Bokobza, L.; Burr, A.; Garnaud, G.; Perrin, M. Y.; Pagnotta, S. Polym Int 2004, 53, 1060.
16. Dogan, M.; Turhan, Y.; Alkan, M.; Namli, H.; Turhan, P.; Demirbaş, O. Desalination 2008, 230, 248.
17. Jia, D.; Liu, J. Q.; Yao, X.; Wang, Y. L. J Wuhan Univ Techn Mater Sci Ed 2004, 19, 44.
18. Hatakeyama, T.; Zhenhai, L. Handbook of Thermal Analysis; Wiley: New York, 1998.
19. Moly, K. Y.; Radusch, H. J.; Androsh, R.; Bhagawan, S. S.; Thomas, S. Eur Polym J 2005, 41, 1410.
20. Kuang, W.; Facey, G. A.; Detellier, C. Clays Clay Min 2004, 52, 635.